High-Resolution Satellite-Derived Dataset of the Surface Fluxes of Heat, Freshwater, and Momentum for the TOGA COARE IOP

J. A. Curry,* C. A. Clayson,[+] W. B. Rossow,[#] R. Reeder,*
Y.-C. Zhang,[@] P. J. Webster,* G. Liu,[&] and R.-S. Sheu[**]

ABSTRACT

An integrated approach is presented for determining from several different satellite datasets all of the components of the tropical sea surface fluxes of heat, freshwater, and momentum. The methodology for obtaining the surface turbulent and radiative fluxes uses physical properties of the atmosphere and surface retrieved from satellite observations as inputs into models of the surface turbulent and radiative flux processes. The precipitation retrieval combines analysis of satellite microwave brightness temperatures with a statistical model employing satellite observations of visible/infrared radiances. A high-resolution dataset has been prepared for the Tropical Ocean Global Atmosphere Coupled Ocean–Atmosphere Response Experiment (TOGA COARE) intensive observation period (IOP), with a spatial resolution of 50 km and temporal resolution of 3 h. The high spatial resolution is needed to resolve the diurnal and mesoscale storm-related variations of the fluxes. The fidelity of the satellite-derived surface fluxes is examined by comparing them with in situ measurements obtained from ships and aircraft during the TOGA COARE IOP and from vertically integrated budgets of heat and freshwater for the atmosphere and ocean. The root-mean-square differences between the satellite-derived and in situ fluxes are dominated by limitations in the satellite sampling; these are reduced when some averaging is done, particularly for the precipitation (which is from a statistical algorithm) and the surface solar radiation (which uses spatially sampled satellite pixels). Nevertheless, the fluxes are determined with a useful accuracy, even at the highest temporal and spatial resolution. By compiling the fluxes at such high resolution, users of the dataset can decide whether and how to average for particular purposes. For example, over time, space, or similar weather events.

1. Introduction

The interaction between the tropical atmosphere and the Pacific Ocean warm pool consists of intense but episodic exchanges of heat, momentum, and freshwater. This coupling of the atmosphere–ocean system occurs over temporal scales ranging from that of an individual cloud to the Walker circulation. A unique feature of the equatorial oceans is the existence of a free-wave mode of large zonal wavelength called an equatorial Kelvin mode that carries energy to the east. These Kelvin waves are partly responsible for the rapid response of the equatorial ocean to atmospheric forcing. Therefore, even mesoscale events that occur in the equatorial regions can create large zonal perturbations. However, the way in which these mesoscale events influence the coupled atmosphere–ocean system on timescales from the mesoscale to the interannual is not well understood.

The Tropical Ocean Global Atmosphere Coupled Ocean–Atmosphere Response Experiment (TOGA COARE) is an observation and modeling program that aims specifically at the elucidation of the physical pro-

*Program in Atmospheric and Oceanic Sciences, University of Colorado, Boulder, Colorado.
[+]Department of Earth and Atmospheric Sciences, Purdue University, West Lafayette, Indiana.
[#]NASA/Goddard Institute for Space Studies, New York, New York.
[@]Department of Applied Physics, Columbia University, New York, New York.
[&]Department of Meteorology, The Florida State University, Tallahassee, Florida.
[**]National Center for Atmospheric Research, Boulder, Colorado.
Corresponding author address: Dr. J. A. Curry, Department of Aerospace Engineering Sciences, Program in Atmospheric and Oceanic Sciences, Engineering Center, Campus Box 429, Boulder, CO 80309-0429.

cesses that determine the mean and transient state of the warm pool region and the manner in which the warm pool region interacts with the global ocean and atmosphere (Webster and Lukas 1992; Godfrey et al. 1998). This program culminated in a major field experiment in the tropical western Pacific Ocean with an intensive observing period (IOP) from November 1992 through March 1993. Central to the scientific objectives of TOGA COARE is the determination and interpretation of the fluxes of heat, moisture, and momentum at the air–sea interface. Fields of surface fluxes for TOGA COARE are needed for the following applications: atmospheric heat and moisture budget studies; forcing for 3D ocean models; evaluation of 3D atmospheric and coupled atmosphere–ocean models; and diagnostic studies related to sea surface temperature, the state of the upper ocean, and feedbacks between the atmosphere and ocean.

A commonly stated goal is that the surface energy balance of the tropical oceans must be known to within 10 W m^{-2} (e.g., Webster and Lukas 1992), implying that the individual component fluxes must be known to accuracy better than 5 W m^{-2}. This is a difficult goal to achieve, even using in situ measurements of surface fluxes, because of instrumentation errors and/or use of ancillary techniques to derive the fluxes from the surface measurements. Additionally, in situ measurements of ocean surface fluxes are very sparse and infrequent; consequently, because of the importance of epoisodic events like westerly wind bursts, sampling errors dominate the uncertainty even for values averaged over large space and time scales. Moreover, such poor sampling limits our understanding of the processes controlling these fluxes by precluding their observation at the scales on which they vary. Hence, it is desirable to determine all of the components of the surface heat, freshwater, and momentum balances from satellite measurements. Satellite observations cover the complete range of variation scales, from mesoscale to planetary-climate scales, but it is a major challenge to infer all of the relevant quantities from satellite observations with the required accuracy at such high resolution. Detailed comparisons between in situ measurements and satellite inferences are necessary to establish this capability.

A critical issue in determining the needed temporal and spatial scales for a satellite dataset in oceanic regions is an understanding of the temporal and spatial scales of surface forcing to which the ocean responds. The tropical western Pacific appears to be inefficient in transporting heat away from the Tropics

by horizontal exchanges; this, in combination with the shallow mixed layer, means that the sea surface temperature is very sensitive to variations in the local surface heat flux between the ocean and the atmosphere. An accurate determination of surface heat flux is therefore clearly important for determining the steady-state temperature and heat content of the western Pacific. In general, the use of monthly mean winds and fluxes provides simulations that are too cold in the eastern Pacific and too warm in the western Pacific (Hayes et al. 1989). Apparently, a shorter time-averaging period for the surface fluxes and/or a proper averaging over nonlinear behavior is needed to reproduce the correct ocean climatology. Are daily averaged values of the surface flux components adequate or must the diurnal cycle of some (or all) of the flux components be resolved? Can weekly values of some of the flux components be used? On what spatial scales must such time variations be resolved? To address these issues, a high-resolution dataset is necessary for diagnostic and modeling studies to test appropriate averaging schemes.

Most previous satellite determinations of one or two components of the sea surface heat fluxes have been made for weekly or monthly timescales. Gautier et al. (1988) and Michael and Nunez (1991) have attempted to retrieve monthly mean values of all of the components of the ocean surface heat flux (i.e., radiative, sensible, and latent heat). Recently, attempts have been made to determine from satellite data the surface flux components on daily timescales or on scales that resolve the diurnal cycle. Chou et al. (1997) and Schulz et al. (1997) have determined daily values of the surface turbulent heat fluxes. Rossow and Zhang (1995) have determined all the components of the surface radiative fluxes on a timescale of 3 h for a spatial scale of 280 km. Sheu et al. (1996, hereafter SCL) derived a mixed satellite precipitation algorithm (microwave, visible, and infrared) that retrieves precipitation on a scale of 50 km and 3 h, although averaging of the pixel-level retrievals is required to take advantage of the statistical nature of the algorithm. Clayson and Curry (1996) determined values of the turbulent fluxes of momentum, sensible, and latent heat on scales of 50 km and 3 h.

In this paper we combine elements from some of the aforementioned studies to produce an integrated dataset of satellite-derived surface flux components in the tropical western Pacific Ocean during the TOGA COARE IOP, with a temporal scale of 3 h and a spatial scale of 50 km. By presenting the fluxes at high resolution, users of the dataset can decide whether and

how to average, for example, over time, space, or similar weather events. In the remainder of the paper, a description of the satellite retrieval techniques is given and the validity of the satellite-derived surface fluxes is examined using in situ measurements obtained during the TOGA COARE IOP. The retrievals are applied to determine the net surface fluxes of heat, freshwater, and momentum during the TOGA COARE IOP. The derived fluxes are then compared with atmospheric heat and water budgets determined from an analysis of rawinsonde data.

2. Datasets

The period and location that have been chosen for this study are coincident with the TOGA COARE IOP during the period November 1992 through February 1993. The focus of the observations presented here is the intensive flux array (IFA), covering a region roughly from 4°S to 2°N and 150°E to 160°E (Fig. 1). The availability of in situ data obtained from ships and aircraft against which to compare the satellite-derived fluxes allows careful determination of errors associated with the satellite fluxes and determination of their causes.

a. Satellite

The satellite datasets used in this analysis are 1) the Defense Meteorological Satellite Program Special Sensor Microwave/Imager (SSM/I) brightness temperatures, 2) the Advanced Very High Resolution Radiometer (AVHRR) infrared radiances, 3) the International Satellite Cloud Climatology Project (ISCCP) cloud analysis results from Geostationary Meteorological Satellite visible and infrared radiances, and 4) the Atlas et al. (1996) surface wind dataset that uses SSM/I data.

The SSM/I (Hollinger et al. 1990) has seven separate total-power radiometers at frequencies of 19.35, 22.235, 37, and 85.5 GHz (hereafter referred to as 19, 22, 37, and 85 GHz). Dual-polarization measurements are taken at 19, 37, and 85 GHz, and only vertical polarization is observed at 22 GHz. The spatial resolution ranges from 69 km × 43 km at 19 GHz to 15 km × 13 km at 85 GHz. The swath width is 1394 km on the earth's surface and the antenna beams intersect the earth's surface at an angle of 53°. In the Tropics the narrow swath results in reduced local coverage. During the period under consideration, data from both the *F10* and *F11* satellites were used, resulting in local coverage in the equatorial oceans of approximately twice per day.
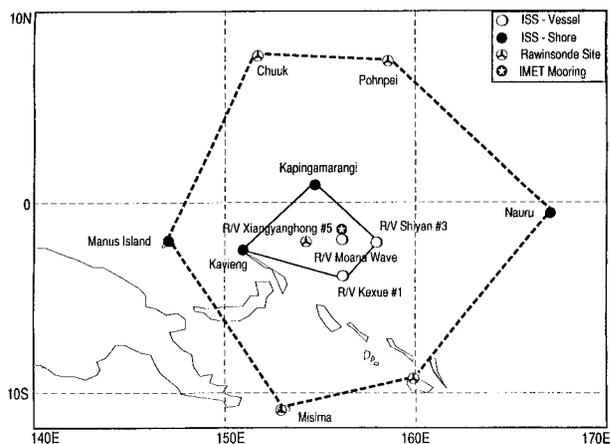

FIG. 1. Map of the TOGA COARE region, indicating the location of major research platforms used in this study. The IFA is bounded (solid line) by Kavieng, Kapingamarangi, R/V *Shiyan* #3, and R/V *Kexue* #1.

The AVHRR is a five-channel scanning radiometer that measures emitted and reflected radiation at visible (0.6 μm), near-infrared (0.9 μm), and thermal infrared (3.7, 10.5, and 11.5 μm) wavelengths. These radiometers are flown on the National Oceanic and Atmospheric Administration (NOAA) polar-orbiting weather satellites; during the TOGA COARE IOP, data from both *NOAA-11* and *NOAA-12* are available. For this study, infrared radiances from the nighttime passes only are converted to weekly average SST values using the MCSST algorithm (McClain et al. 1985). The final SSTs (described in section 3a) are determined using these weekly mean values.

A special high-resolution ISCCP analysis (DX) was prepared for the TOGA COARE IOP (see Rossow et al. 1996). To reduce data volume the ISCCP data are sampled with a temporal sampling interval of 3 h and a spatial sampling interval of approximately 30 km; thus about 1 in 30 pixels is available to represent a region about 30 km in size. The ISCCP analysis procedure determines values of the surface visible reflectance and SST and, for each cloudy pixel, the cloud-top temperature/pressure and visible optical thickness.

The Atlas et al. (1996) wind dataset uses an optimal interpolation method to determine wind speeds and directions using a combination of model output, in situ measurements, and SSM/I-derived wind speeds. The spatial resolution of the dataset is 250 km and the temporal resolution is 6 h.

b. In situ data

The principal ship dataset used for validation in this study is obtained from the R/V *Moana Wave* (Fig. 1).

The R/V *Moana Wave* obtained measurements during three separate cruises in the period 11 November through 16 February (Young et al. 1995; Fairall et al. 1996a,b). Mean and perturbation wind and temperature measurements were made using a sonic anemometer. A dual-wavelength infrared hygrometer was used to measure both mean and perturbation humidity. SST was measured using a thermistor sealed in the top of a floating hose, measuring the temperature at a depth of approximately 5 cm. Surface radiation fluxes were measured using an Eppley pyranometer and pyrgeometer. Precipitation was measured using an optical rain gauge. The version of the R/V *Moana Wave* flux dataset used in this study consisted of hourly averaged values. Data from additional ships and from the Improved Meteorological (IMET) buoy are also used in various aspects of the intercomparison with the satellite-derived fluxes. The efforts undertaken by oceanographers to calibrate the instruments and conduct intercomparisons between instruments on different platforms are summarized by Godfrey et al. (1998).

The aircraft dataset used for comparison in this study comes from measurements made by two NOAA WP-3D aircraft flying during the TOGA COARE IOP. The data from flights during 10 February 1993 have been gridded and surface fluxes calculated for an area of approximately 1.5° in latitude by 3.0° in longitude just outside the IFA region (Geldmeier and Barnes 1997). The data were gridded to a resolution of 11 km, and surface turbulent fluxes were calculated using the TOGA COARE bulk flux algorithm (Fairall et al. 1996a).

3. Description of satellite flux algorithms

The net fluxes of heat, freshwater, and momentum into the ocean surface can be written as the sum of several component contributions. The net heat flux into the ocean surface, H_{net} (W m^{-2}), is given by

$$H_{net} = H_{rad} + H_S + H_L + H_{PR}, \qquad (1)$$

where H_{rad} represents the net surface radiation flux, H_S refers to the surface turbulent flux of sensible heat, H_L is the surface turbulent flux of latent heat, and H_{PR} is the heat transfer by precipitation. Note that the sign convention here, with positive heat flux into the ocean, is opposite to that typically used by meteorologists. The terms on the right-hand side of (1) are the surface heat flux components that are evaluated here. A heat flux component is positive if it is a source of heat for the ocean.

Analogous to (1), we can write the net freshwater flux into the ocean surface, F, in units of mm day^{-1} as

$$F_{net} = P - E, \qquad (2)$$

where P is the rainfall rate and E is the evaporative flux of water from the ocean surface. The evaporative flux E is related to H_L by $E = -H_L/\rho L$, where L is the latent heat of vaporization and ρ is the density of water. The freshwater flux into the ocean is positive if the magnitude of precipitation exceeds that of evaporation.

We write the flux of momentum into the ocean surface, M_{net} (N m^{-2}), as

$$M_{net} = \tau_a + \tau_P, \qquad (3)$$

where we ignore the momentum flux radiated out by propagating surface waves. The term τ_a is the shear stress applied by the atmosphere to the ocean and τ_P is the momentum flux associated with precipitation.

In determining the surface fluxes of heat, freshwater, and momentum, we evaluate each of the component fluxes on the right-hand sides of (1)–(3). Although methods have been proposed to determine directly the net surface heat flux (e.g., Suomi et al. 1996), we prefer to calculate the individual components since these are more useful in diagnostic studies than the net flux itself.

Description of the methodology for obtaining the surface flux components from satellite observations is divided into sections on radiative fluxes, precipitation fluxes, and turbulent fluxes. Within each section, determination of the necessary input variables is described.

a. Radiation fluxes

The net surface radiation flux into the surface, H_{rad} (W m^{-2}), can be represented as the sum of the net shortwave (SW = 0.2–5.0 μm wavelengths) and net longwave (LW = 5.0–200 μm) fluxes:

$$H_{rad} = (1 - \alpha)H_{SW} + [1 - (1 - \varepsilon)]H_{LW} - \varepsilon\sigma T_0^4, \quad (4)$$

where H_{SW} is the downwelling solar (shortwave) radiation flux at the surface, α is the surface albedo, H_{LW} is the downwelling thermal infrared (longwave) radiation flux at the surface, T_0 is the surface temperature, ε is the surface emissivity, and $(1 - \varepsilon)$ is the surface longwave reflectivity.

Many simple methods for calculation of the components of the surface fluxes from satellite observations have been described (e.g., Pinker and Ewing 1985; Bishop and Rossow 1991; Chou et al. 1998). However, for this study we use a complete radiative transfer model with retrieved physical variables as inputs to obtain a physically consistent relation between all radiative flux components and to allow for a diagnosis of flux variations in terms of the variations of these physical variables. The same model is also used to determine the radiative fluxes at the top of the atmosphere (in this case, taken to be the 100-mb level) for the heat budget calculations in section 5a. Following Zhang et al. (1995), all radiative flux components are calculated using a modified version of the radiative transfer model from the National Aeronautics and Space Administration/Goddard Institute for Space Studies (NASA/GISS) GCM. In this procedure satellite data are analyzed to retrieve most of the physical variables that determine radiative transfer in the atmosphere, particularly clouds, water vapor, and temperature. The model accounts for the full wavelength and angle dependence of radiation caused by absorption of atmospheric gases, clouds, and the surface and by multiple scattering from gases, aerosols, the surface, and clouds. The resulting flux values represent 3-h averages centered on the synoptic observation times (0000, 0300, 0600 UTC, etc.).

There are important differences between the full radiative model calculations and (4). In the model, both α and ε are wavelength-dependent quantities; hence, the upwelling shortwave flux is not strictly proportional to H_{SW} and the upwelling longwave flux is not strictly proportional to T_0^4. Moreover, with surface emissivity less than unity, the downwelling longwave flux from the atmosphere into the ocean is reduced by the reflection of H_{LW} from the surface (where the effective longwave albedo is given approximately by $1 - \varepsilon$); this reflected longwave flux is often neglected, but it can be as large as the reflected shortwave flux. Also, the net shortwave is not simply given by the difference between H_{SW} transmitted through the atmosphere and a flux reflected from the surface, as represented by the factor $(1 - \alpha)$, because there are multiple reflections between the atmosphere, clouds, and surface that are wavelength dependent. The radiative model calculations account for these wavelength dependencies (Zhang et al. 1995).

Our treatment differs from Zhang et al. (1995) in a number of ways, including improved treatments of the water vapor continuum (based on Ma and Tipping 1994), aerosols, surface albedos and emissivities, cloud microphysical properties, effects of solar zenith angle variations, and increased spectral resolution. The main new feature of our treatment exploits changes in the ISCCP retrievals of cloud-top temperature (T_c) and visible optical thickness (τ) that explicitly treat liquid and ice clouds with different microphysical models (Rossow and Schiffer 1999). The ISCCP retrieval now treats ice clouds ($T_c < 260$ K) as composed of ice polycrystals, with effective radii of ice and liquid clouds specified consistent with the analyses of Han et al. (1994) and Han et al. (1994). Cloud-layer thicknesses are specified by a more extensive climatology of cloud-layer structure obtained from an analysis of 20 years of rawinsonde humidity profiles (Wang et al. 1999, manuscript submitted to *J. Climate,* hereafter WRZ). The number of cloud layers (1–3) is determined by the total cloud optical depth, with the depth of an individual layer and top of the lower layers specified following the tropical ocean results from the climatology of WRZ. The new radiative flux calculations, like the new ISCCP retrievals, now use different microphysical models for liquid and ice clouds.

The ocean surface albedo follows the wavelength and angular dependence specified in an improved version for the GISS GCM, which accounts for Fresnel reflection from a wind-roughened surface, surface foam at high wind speeds, and a fixed amount of volume scattering by hydrosols. This model gives a wavelength-averaged surface albedo for the ocean near the equator of about 0.063 (calculated as the ratio of the daily mean upwelling to downwelling shortwave fluxes), similar to the value of 0.058 determined from measurements from the R/V *Franklin* (F. Bradley 1997, personal communication).

In place of the Television Infrared Observation Satellite Operational Vertical Sounder (TOVS) atmospheric profiles (used in the ISCCP analysis), for the TOGA COARE IOP we use the rawinsonde-based atmospheric profiles of temperature and humidity, obtained every 6 h during the IOP and interpolated to 3-h intervals (Johnson et al. 1996). This change significantly reduced the bias between the calculated and measured downwelling longwave fluxes. Moreover, instead of assuming the same humidity profile for clear and cloudy atmospheric columns, the water vapor mixing ratio in all cloud layers is increased to saturation. Stratospheric aerosol optical thickness accounts for the effect of the decaying Mount Pinatubo volcanic aerosol: optical thickness decreases from 0.084 in November 1992 to 0.0538 in February 1993 (Hansen et al. 1997). The amount and composition of the tro-

pospheric aerosol in the TOGA COARE region is poorly known; here we adopt a value of tropospheric aerosol optical thickness of 0.11, based on sunphotometer measurements at Kavieng (C. Long 1997, personal communication).

SKIN SEA SURFACE TEMPERATURE

The radiative, latent, and sensible heat exchanges between the atmospheric and oceanic boundary layers all depend on the actual "skin" temperature of the ocean, which may differ by several degrees from the bulk sea surface temperature measured by buoys or ships at depths from 0.5 to 10 m below the surface (e.g., Schluessel et al. 1990). As calculated by Webster et al. (1996), an error of 1°C in the SST results in an error of 19 W m^{-2} in the surface latent heat flux for mean conditions during TOGA COARE. Zhang et al. (1995) show that a similar error in SST causes an error of about 10 W m^{-2} in the upwelling longwave radiative flux.

Sea surface temperature determination from infrared satellite measurements can be interpreted directly in terms of this skin temperature, although most methods of satellite sea surface temperature retrieval have been regressed to reproduce bulk temperatures for comparison with in situ bulk temperature measurements made by ships and buoys (e.g., Reynolds and Marsico 1993). Infrared methods of satellite sea surface temperature determination are limited to clear-sky conditions. Persistently cloudy conditions and very large water vapor abundances make SST retrievals in the tropical western Pacific particularly challenging.

The approach used here to determine the skin sea surface temperature follows Clayson and Curry (1996). First, a value of the predawn skin SST is obtained by using the weekly MCSST analyses and linearly interpolating these values to form a daily time series. A skin temperature correction that is dependent on wind speed is added to determine the predawn skin temperature. Then a diurnal cycle of skin temperature is superimposed to form a time series with 3-h resolution. For each day, the amplitude of the diurnal cycle is determined using the model results described by Webster et al. (1996), where this amplitude is determined to be a function of the daily peak solar insolation, the daily averaged precipitation, and the daily averaged surface wind speed. The amplitude of the diurnal cycle, when added to the predawn skin SST, determines the skin SST at local noon; skin SST values at other times are determined by fitting a half-cosine curve to the times of local dawn and dusk and the noon value of skin SST. There are several required

satellite-derived input variables to determine the time series of skin temperature. These include the interpolated MCSST dataset (section 2a) and surface winds [section 3b(1)] to determine the predawn skin correction to the MCSST values. To determine the amplitude of the diurnal cycle, we need the daily averaged wind speed [section 3b(1)], peak solar insolation (in section 3a), and daily averaged precipitation (section 3c). When compared with instantaneous observations obtained from the R/V *Moana Wave,* it was shown by Clayson and Curry (1996) that the bias of the satellite-derived skin temperature values is 0.08°C relative to the ship values, with an rms error of 0.34°C and a correlation coefficient of 0.75.

b. *Turbulent fluxes*

The general technique used to determine the surface turbulent fluxes of momentum and sensible and latent heat follows Clayson and Curry (1996), with two changes. The basis for this technique is the bulk turbulence flux model described by Clayson et al. (1996). We have modified the turbulence flux model to include the Webb et al. (1980) correction for the latent heat flux. The so-called Webb correction addresses the requirement that the net dry mass flux be zero, and has an average magnitude of 4 W m^{-2} for the TOGA COARE data (Fairall et al. 1996a). In applying the bulk turbulent flux model over a region of spatial scale 50 km and temporal scale of 3 h, it is important to account for the mesoscale variability of the surface fluxes induced by convection. Jabouille et al. (1996) used a cloud-resolving model to simulate convection over a domain with a scale of 90 km. They found that adding in quadrature a gustiness velocity to the mean wind improved evaluation of the surface fluxes. The magnitude of the gustiness velocity is parameterized following Jabouille et al. (1996) to be 0.5 m s^{-1} in nonconvective conditions (no rainfall), and up to 3 m s^{-1} when deep convection is present (as indicated by rainfall rate of 1 mm h^{-1} or higher). The gustiness parameterization increases the magnitude of the IFA-averaged latent heat flux by 4.8 W m^{-2}, the sensible heat flux by 0.4 W m^{-2}, and the momentum flux by 0.01 N m^{-2}, relative to calculations without including the gustiness parameterization.

To use the bulk turbulence flux model to determine the surface fluxes of sensible and latent heat and momentum from satellite, the following input parameters are required: 10-m surface wind speed (u_a), atmospheric temperature (T_a), and humidity (q_a), and also the skin SST (T_0) and sea surface specific humidity (q_0).

1) SURFACE WIND SPEED

In this study, surface wind speed is determined using SSM/I data from the *F10* and *F11* satellites, following Clayson and Curry (1996). This algorithm was developed by regressing the SSM/I brightness temperatures against 69 ship observations of surface wind speed measured by the R/V *Franklin.* Because of the large influence of precipitation on the SSM/I brightness temperatures and the sea state, surface wind speeds cannot be determined from SSM/I brightness temperatures when it is raining. When compared with instantaneous observations obtained from the R/V *Moana Wave,* it was shown by Clayson and Curry (1996) that the bias of the satellite-derived wind speeds is very small, the satellite-derived value of the mean surface wind speed being 0.07 m s^{-1} greater than the ship values. The rms error is 1.55 m s^{-1} and the correlation between the two datasets is 0.79.

Since SSM/I coverage in the Tropics is only twice per day and wind speeds cannot be determined when it is raining, substantial gaps exist in a time series of surface wind speed determined from SSM/I. Clayson and Curry (1996) dealt with gaps in the SSM/I wind speed data using an interpolation scheme. Here we use the Atlas et al. (1996) winds dataset, where we have linearly interpolatedthis dataset down from 250 km and 6 h to 50 km and 3 h. The final surface wind speed dataset consists of coincident SSM/I winds when available, supplemented by the Atlas et al. (1996) winds when the SSM/I winds are not available.

2) SURFACE AIR TEMPERATURE

Our parameterization of $T_a - T_0$ follows Clayson and Curry (1996) and is based on the hypothesis that atmospheric surface layer static stability is reflected by the type of clouds present. A simplified version of the Liu et al. (1995) tropical cloud classification scheme is used, which includes the cloud-top temperature, whether or not it is precipitating, and whether it is day or night. The differences between the classes were compared to determine those differences that were statistically significant at the 99% level. Seven different categories were distinguished, each associated with a characteristic value of $T_a - T_0$.

The satellite-derived input values required for the cloud classification scheme are cloud-top temperature (derived from the ISCCP dataset) and whether or not it is precipitating (determined in section 3c). When compared with instantaneous observations obtained from the R/V *Moana Wave,* it was shown by Clayson and Curry (1996) that the mean bias in the satellite-derived T_a relative to the ship-measured T_a is 0.12°C, the rms error is 0.77°C, and the correlation is 0.67.

3) SURFACE AND AIR SPECIFIC HUMIDITY

Values of the saturation specific humidity at the surface (q_0) are easily determined once a value of surface temperature is known. Once T_0 has been determined, a value of q_0 is determined from $q_0 = 0.98 q_s(T_0)$, where q_s is the saturation vapor pressure. This expression accounts for the reduction in saturation vapor pressure associated with a surface salinity of 34 psu.

Values of the water vapor mixing ratio in the atmospheric surface layer (q_a) are not available directly from satellite analyses, since the retrievals from TOVS and other satellite sounders that are currently available do not have sufficient vertical resolution. Several methods have been proposed for determination of q_a; for the reasons outlined in Clayson and Curry (1996) we use the algorithm described here. This algorithm follows the general approach described by Miller and Katsaros (1992). An expression for $q_a - q_0$ is determined from a regression of the ship values versus satellite-derived values of T_0, precipitable water (W), and surface wind speed (u_a). Satellite-derived values of W are determined using SSM/I data and the algorithm of Schluessel and Emery (1990), which was shown by Sheu and Liu (1995) to have the highest correlation with values of W derived from radiosonde data during the TOGA COARE IOP. We note here that the Clayson and Curry (1996) algorithm is applicable only for tropical oceans and should not be applied outside this region. The input data depend on the SSM/I data, so direct retrievals are only available approximately twice per day.

c. Precipitation

Numerous satellite rainfall algorithms have been developed and evaluated over the tropical oceans, in the context of the Global Precipitation Climatology Project Algorithm Intercomparison Project (AIP-3) (Ebert and Manton 1998) and the NASA WetNet Precipitation Intercomparison Project (PIP) (Smith et al. 1998). In the tropical oceans, the AIP-3 used shipborne radar as the evaluation dataset and PIP-3 used the atoll rain gauge dataset. One of the frustrating aspects of the evaluation of the satellite rainfall algorithms is that a majority of the algorithms had a negative bias relative to the atoll data, but a positive bias relative to the radar data. Although there was not an exact overlap of algorithms used in the two studies, this difference needs to be addressed before the community can be

confident of the absolute magnitude of the rainfall estimates (R. Adler 1997, personal communication). According to Godfrey et al. (1998), a 25% uncertainty remains in the surface-based precipitation estimates during TOGA COARE.

In this study, we adopt a mixed rainfall algorithm following SCL. This algorithm combines the advantages of both the ample coverage of visible/infrared (VIS/IR) sampling and the physical link between precipitation and microwave radiances. A VIS/IR algorithm is trained using SSM/I-derived values of precipitation. Cloud-top temperatures and visible optical depth provided by the ISCCP DX analyses are binned by every 10 K and every 10-unit optical depth, respectively. Lookup tables for the probability of rain and mean rainfall rate are constructed for each cloud-top temperature/optical depth cell whenever the optical depth is available (daytime). For nighttime, the tables are based only on cloud-top temperature. The instantaneous rainfall rates are obtained by multiplying the mean rainfall rate by the probability of rain for the cell in which cloud-top temperature and/or visible optical depth reside. The final algorithm uses SSM/I when available; otherwise the VIS/IR algorithm is used during the day and the IR algorithm at night. The Sheu et al. mixed algorithm overestimates the rainfall relative to the radar data (Ebert and Manton 1998; SCL), and slightly underestimates the rainfall relative to surface rain gauge measurements. Here, the mixed algorithm of Sheu et al. is retrained using a revised rain threshold for the SSM/I algorithm that varies with monthly SST climatology, which reflects regional variations in the height of freezing level and the amount of water vapor. Because of the change in rain threshold, more light rainfall events were retrieved in the TOGA COARE region compared to SCL. The original Sheu et al. rainfall algorithm yields an average rainfall of 6.0 mm day^{-1} for the TOGA COARE IFA, while the new mixed algorithm yields an average rainfall of 8.3 mm day^{-1}. Because of the statistical nature of the relationship, averaging (either in space or time) improves the results, with more averaging required for the IR algorithm to achieve an accuracy comparable to the VIS/IR algorithm.

1) SENSIBLE HEAT FLUX OF RAIN

The term H_{PR} in (1) is the sensible heat flux at the surface due to rain. Heat transfer by precipitation can occur if the precipitation is at a different temperature than the surface. Following Gosnell et al. (1995), we assume that a falling raindrop is in thermal equilibrium

with its surroundings, with a temperature corresponding to the wet-bulb temperature of the atmosphere at that height. Assuming that the temperature of the rain as it hits the ocean surface is equivalent to the wet-bulb temperature of the atmosphere just above the surface, T_w, we can write

$$Q_{\mathrm{PR}} = \rho c_p P(T_w - T_0),\qquad(5)$$

where ρ and c_p refer to the liquid water values and P is the rainfall rate in units of m s^{-1}. Values of H_{PR} are greatest for large rainfall rates and for large differences between the atmospheric wet-bulb temperature and sea surface temperature. During heavy rainfall events, values of H_{PR} may be the largest term in the surface energy budget; however, when H_{PR} is averaged over longer timescales, the contribution of this term to the surface energy budget is quite small and is commonly neglected. Since our focus is on high-resolution surface fluxes, we retain this term in our analysis. To evaluate Q_{PR} using satellite observations, the required inputs are rainfall rate, the surface temperature T_0, [section 3a(3)], and the surface atmospheric wet-bulb temperature T_w, which is determined from retrieved values of T_a and q_a following sections 3b(2) and 3b(3).

2) MOMENTUM FLUX OF RAIN

The momentum flux due to rain arises from the fact that the raindrops carry horizontal momentum at the time of their impact with the ocean. We calculate the momentum flux of rain, τ_p, following Caldwell and Elliot (1971), from

$$\tau_p = 0.85\,\rho P u_a.\qquad(6)$$

The constant 0.85 is chosen as an approximation of the average reduction in drop speed of 15% from the wind speed. As with the sensible heat flux from rain, the momentum flux due to rain is only an important component of the overall momentum flux during periods of locally heavy rain. During these time periods the momentum flux due to rain can be 50% of the total momentum flux, although this contribution is less important when averaged over larger temporal and spatial scales.

d. Assembly of satellite flux dataset

All data from satellite and ancillary datasets are collected into 0.5° longitude and latitude bins, every 3 h. If a specific input variable for one of the flux algorithms is missing for a specific bin at a given time,

then a space–time interpolation scheme is used to fill in the missing values. A complete gridded dataset of input variables is then used to calculate the component fluxes at a resolution of 0.5° and 3 h. Following Clayson and Curry (1996), we find it preferable to interpolate the input data rather than to interpolate the fluxes themselves.

4. Comparison of satellite-derived fluxes with other datasets

The satellite-derived fluxes are compared here with in situ and aircraft observations of surface fluxes. In spite of the mismatch in scales being considered, especially with fluxes measured from a ship, such comparisons are useful for evaluating the satellite-derived fluxes. The satellite fluxes, in turn, are better than surface observations for evaluating fluxes produced by numerical weather prediction centers because of the closer match in spatial sampling and coverage.

a. Comparison with ship data

Comparisons of the satellite-derived and the in situ ship data are shown in Table 1. The in situ turbulence flux data are determined from the eddy covariance measurements. The interpolated 3-hourly data in the 0.5° cell nearest the ship location are compared with the ship data during the cruise period; daily and 5-day averages based on the 3-hourly satellite data and the in situ ship daily averages are also shown.

Discrepancies between the satellite-derived fluxes and the in situ ship measurements may be caused by bias in the surface-based flux observations, errors in

TABLE 1. Comparison of 3-hourly, daily averaged, and 5-day averaged surface flux components determined from in situ measurements on the R/V *Moana Wave* and from satellite (0.5° × 0.5° grid cell). Positive values indicate flux into the ocean.

	Net shortwave flux (W m^{-2})	Net longwave flux (W m^{-2})	Latent heat flux (W m^{-2})	Sensible heat flux (W m^{-2})	Momentum flux (N m^{-2})	Precipitation (mm h^{-1})
Three-hourly values						
Satellite mean	209	−45	−127	−6	0.070	0.39
Ship mean	183	−53	−107	−10	0.056	0.45
Bias (ship–satellite)	−26	−8	19	−4	−0.014	0.06
Satellite std dev	287	13	58	7.3	0.08	1.06
Ship std dev	252	11	49	11	0.137	1.55
Rms error (ship–satellite)	86	16	45	11	0.133	1.63
Correlation	0.96	0.35	0.72	0.37	0.34	0.26
Daily values						
Rms error (ship–satellite)	35	11	33	7	0.089	0.66
Correlation	0.93	0.68	0.84	0.59	0.52	0.59
Five-day values						
Rms error (ship–satellite)	25	9	25	5	0.043	0.31
Correlation	0.99	0.89	0.95	0.73	0.76	0.75

the satellite-derived values, or differences in spatial and temporal sampling and coverage. Estimates of ship measurement bias errors of individual heat flux components are 3 W m^{-2} for shortwave flux, 2 W m^{-2} for longwave flux (Weller and Anderson 1996), and 4 and 2 W m^{-2}, respectively, for the latent and sensible heat fluxes (Fairall et al. 1997). The biases in radiation flux measurements were determined from intercomparison of measurements made from different platforms in essentially the same location; however, we note that comparison between the satellite-based results and surface measurements from other sites over a larger area suggests that larger bias errors (as much as 20 W m^{-2} in the shortwave and 10 W m^{-2} in the longwave) may still be possible. Cess et al. (1999, manuscript submitted to *J. Geophys. Res.*) summarize potential errors in pyranometer measurements of surface solar radiation fluxes, caused by cosine response errors under overcast (diffuse illumination) or broken cloud conditions and by disequilibrium between the temperatures of the filter dome and the detector (Bush et al. 1999). The uncertainty in the solar flux measurements is exacerbated by ship and buoy motions (Katsaros and De Vault 1986) since the instruments were not gimballed to maintain a level position. While quantitative estimates of these errors are not available for the TOGA COARE measurements, it is not difficult to imagine that bias errors in the surface shortwave radiation flux may exceed 10 W m^{-2} owing to these uncertainties.

Biases between the satellite-derived and in situ measurements of heat flux components all exceed the estimated bias errors in the ship measurements. Comparison of the rms error of the 3-hourly satellite fluxes with the observed standard deviation of the ship fluxes shows that rms error of the satellite fluxes is smaller than the observed standard deviation for fluxes of net shortwave radiation and latent heat, and momentum. Together with the high time correlations, this suggests that the satellite-derived fluxes are capturing the spatial and temporal variations of the fluxes accurately despite the systematic difference with in situ measurements. Rms errors of the net longwave radiation flux, sensible heat flux, and precipitation are comparable to or slightly larger than the standard deviations of the in situ data, suggesting that these signals are influenced more by measurement error, although there is still some correlation for these fluxes. When compared with the fluxes with 3-h resolution, the daily and 5-day averaged flux values show increasingly smaller rms errors and higher correlations. Rossow and Zhang (1995) showed that this behavior for the shortwave

radiative fluxes is caused by the sampling of the variable cloud properties. Applications of the dataset that allow averaging in space, time, or over weather events improve the precision of the satellite fluxes.

We note here that the satellite-derived values of the flux components show slightly poorer agreement with the data from the R/V *Moana Wave* than previously reported (e.g., Clayson and Curry 1996). This arises for several reasons. Some changes have been made to the analyses of both the in situ fluxes and the satellite algorithms for some of the input variables. Additionally, the location of the R/V *Moana Wave* is near the corner of one of the grid boxes, while our previous analyses selected the satellite pixels most nearly centered over the ship location. Comparisons between the satellite-derived surface fluxes and the ship-based point measurements illustrate the difficulty of comparing the two datsets, arising from the different space–time sampling of a highly variable quantity (particularly for the downwelling shortwave radiation and precipitation), that are associated with fluctuations in cloud characteristics. Note that using the pixel most nearly centered over the R/V *Moana Wave* reduces the radiation biases to 22.2 and 5.2 W m^{-2} for shortwave and longwave fluxes, respectively, and the respective rms differences are reduced to 54.5 and 8.5 W m^{-2}.

It is a common procedure (e.g., Chou et al. 1998) to tune satellite-derived fluxes to eliminate bias errors. While some of the input variables to the turbulent flux model have been determined from empirical algorithms, here we determine the fluxes using physically based models and, hence, the flux components are not tuned to the observations in any way. We prefer to retain the full understanding of our retrievals made possible using the physically based algorithms, which allows for improvements of the physics or exploitations of new information. We do not have sufficient confidence in the accuracy of the in situ flux measurements (especially the radiation and precipitation fluxes) or of the spatial representativeness of the in situ measurements to justify tuning the satellite-derived flux values. We note here that Chou et al. (1998) have used an empirical method to determine surface shortwave and longwave radiation fluxes from satellite for TOGA COARE, by regressing satellite observations to surface in situ measurements. When compared on a pixel basis with measurements from the IMET buoy (Fig. 1), Chou et al. found a bias and rms difference of 6.2 and 25.5 W m^{-2}, respectively, for the shortwave fluxes and a bias and rms difference of 0.4 and 5.2 W m^{-2} respectively, for longwave fluxes. The sen-

sitivity studies of Zhang et al. (1995) show that such empirical relations between top-of-atmosphere and surface radiation can represent the variability of surface shortwave fluxes quite well; however, in the Tropics, there is almost no relationship between variations of top-of-atmosphere and surface longwave fluxes. Apparently good agreement can be obtained simply because the variation of the surface longwave fluxes in the Tropics is so small.

b. Comparison with aircraft data

The capability of the satellite-derived surface fluxes to capture the horizontal variability associated with a case characterized by a mesoscale convective system (MCS) is illustrated in Fig. 2. The satellite-derived fluxes are compared with fluxes determined from two NOAA WP-3D aircraft that flew over the region 6°–4.5°S and 158°–161°E on 10 February 1993 at an altitude of about 38 m (Geldmeier and Barnes 1997). Although this region is not within the IFA, we have extended the domain of our satellite flux calculations to include this domain and time period. The aircraft data were obtained during a 3-h time period; the satellite-derived fluxes use only the data from the 3-h interpolated time that falls within this 3-h time period.

As documented by Geldmeier and Barnes (1997), the aircraft flew under the anvil region of a decaying MCS, with active convection ending 5–8 h prior to the sample time. The north-central area of Fig. 2 was the last portion to be affected by the MCS leading edge, with areas to the south and east affected previously. The extreme northeast corner has been modified by a recent squall line that formed to the north of the map and moved quickly east. The atmosphere in the wake of the decaying MCS was 2°C cooler and 0.5 g kg^{-1} drier than the undisturbed environment. Latent heat and momentum fluxes in the eastern portion of the map are seen in Fig. 2 to be more than double the values found in the nearby undisturbed environment (western portion). The agreement of the satellite- and aircraft-derived fluxes is very good, with the satellite capturing both the mean value and the spatial variability of the fluxes.

c. Comparison with the ECMWF fluxes

An additional source of surface flux estimates in the TOGA COARE region is the European Centre for Medium-Range Weather Forecasts (ECMWF) reanalysis dataset, which includes surface fluxes produced by the model physics from the initialized analysis. This information is available four times per day at a spatial resolution of 2.5°. Figure 3 and Table 2
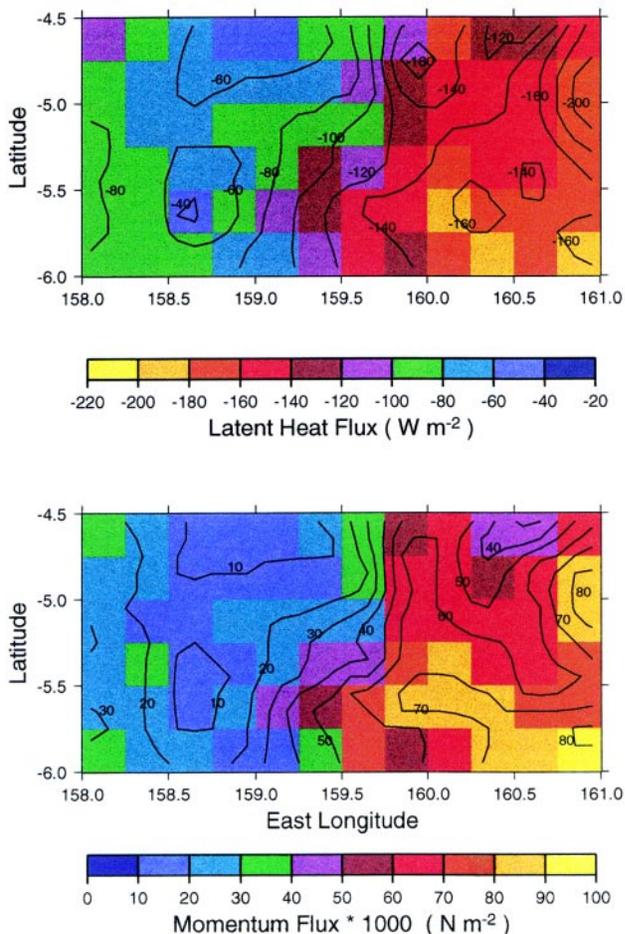

FIG. 2. Comparison of aircraft- and satellite-derived values on 10 Feb 1993 for (a) surface latent heat flux and (b) surface turbulent momentum flux. Contours represent analysis of the aircraft data and colored boxes represent the pixel-level satellite-derived values.

show a comparison of the ECMWF fluxes with the satellite-derived IOP values for the model grid cell centered at 1.25°S, 153.75°E. This comparison illustrates the utility of the satellite flux dataset in evaluating the fluxes produced by numerical weather prediction models, whereby the better match in spatial scales between the model grid and satellite data allows for a more accurate comparison than does a single point measurement.

Table 2 compares the ECMWF values of net shortwave and longwave fluxes, latent heat flux, momentum flux, and precipitation rate with the satellite-derived values. For calculation of the means, rms error, and correlations of the shortwave fluxes only, the daily averaged values were used. The mean modeled momentum flux is only slightly more than half the satellite-derived value, which tends to be smaller than the ship-based values. The mean modeled shortwave flux
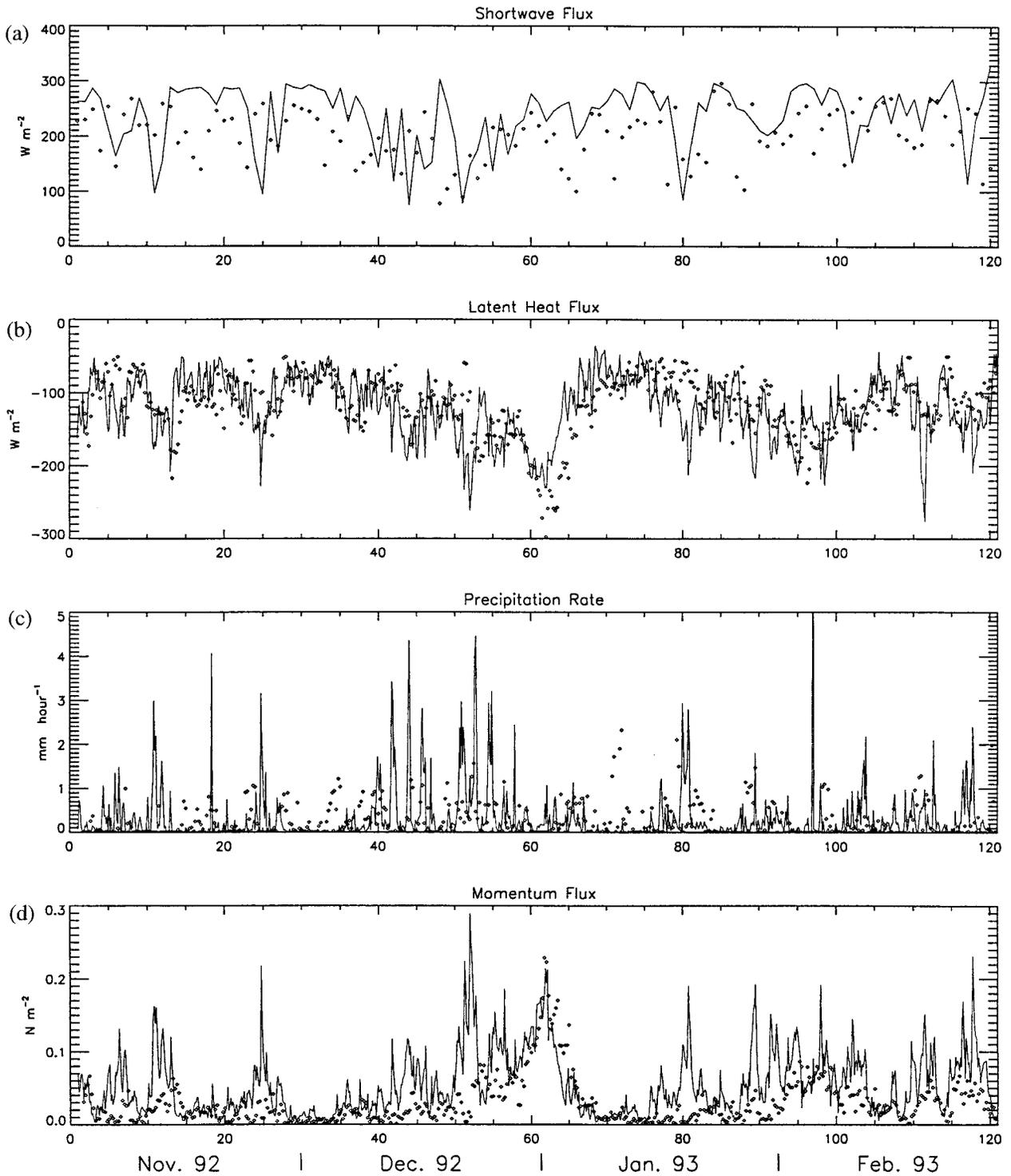
FIG. 3. Time series of IOP comparing satellite and ECMWF fluxes of (a) daily averaged shortwave flux, (b) latent heat flux, (c) precipitation, and (d) turbulent momentum flux. Satellite-derived values are shown by solid lines and ECMWF values are shown by diamonds.

is lower and the net longwave flux is more negative than the satellite-derived values, indicating discrepancies that cannot be explained only by differences in cloud optical depth but might include surface albedo, aerosol properties, and the radiative transfer models. Agreement of the mean modeled and satellite values of sensible and latent heat flux is quite good, although the correlations are not very high. In general, the corre-

TABLE 2. Comparison of satellite-derived fluxes with ECMWF reanalysis fluxes during the TOGA COARE IOP for the model grid cell centered at 1.25°S, 153.75°E. Positive values indicate flux into the ocean.

	Net shortwave flux (W m^{-2})	Net longwave flux (W m^{-2})	Latent heat flux (W m^{-2})	Sensible heat flux (W m^{-2})	Momentum flux (N m^{-2})	Precipitation (mm h^{-1})
Mean satellite	238	−34	−112	−5.0	0.046	0.32
Mean ECMWF	201	−49	−117	−5.1	0.030	0.25
Rms error (ECMWF-satellite)	79	19	40	4.5	0.036	0.66
Correlation	0.09	0.12	0.54	0.14	0.58	0.03

lation between the two precipitation datasets is very small, with the ECMWF mean precipitation value nearly 0.07 mm h^{-1} smaller than the satellite-derived value.

Further insight into the discrepancies between ECMWF and the satellite derived fluxes can be gleaned from Fig. 3, which shows a time series comparison of net shortwave flux, latent heat flux, momentum flux, and precipitation rate. The bias in momentum flux arises from ECMWF missing relatively short-lived, high–wind speed events. Note that during the period of a prolonged westerly wind burst in late December and early January, the high wind speeds are captured by ECMWF, but also note the substantial overestimation by ECMWF of the latent heat flux during this period. In general, the ECMWF shortwave flux is higher than the satellite-derived shortwave flux during cloudier conditions and lower during clear conditions, which is caused by differences in aerosols, humidity profiles, and persistent cirrus cloud.

Weller and Anderson (1996) performed a comparison of the same ECMWF model grid cell with fluxes obtained from the IMET buoy during the IOP. While the results of the Weller and Anderson intercomparison are qualitatively similar to the comparison presented here, we note that the better match in spatial scales between the ECMWF model grid and the satellite data allows for a comprehensive comparison with numerical weather prediction model analyses.

5. Net surface heat, freshwater, and momentum fluxes

A principal goal of TOGA COARE was to determine the net fluxes of heat, freshwater, and momen-

tum over the IFA during the IOP using datasets that would resolve the shorter timescale variability associated with this region. In this section, we describe the results of the satellite-derived surface fluxes averaged over the entire IFA region throughout the IOP.

Table 3 presents the results of the satellite-derived surface fluxes averaged over the IFA and during the four-month period of the IOP (1 November–28 February). The net surface heat flux (positive) is dominated by the net radiation flux (positive) and the latent heat flux (negative). The net freshwater flux is positive, indicating substantial freshening of the ocean. The net momentum flux is determined almost entirely by the turbulent momentum flux.

Figures 4–6 show time series for IFA- and daily averaged values of the satellite-derived component fluxes and net fluxes of heat, freshwater, and momentum. For comparison, the time series of surface meteorology and surface fluxes during the IOP are described by Weller and Anderson (1996) using in situ measurements. During the period before 10 December, the IFA was characterized by low surface wind speeds (as shown by the turbulent momentum flux in Fig. 6), generally high values of the net surface radiation flux (Fig. 4), and generally low values of precipitation (Fig. 5), resulting in a generally positive net heat flux of a little less than 100 W m^{-2}. Starting on 10 December and continuing to the end of the month, a westerly wind burst event occurred, associated with enhanced turbulent momentum and latent heat fluxes, increased rainfall, and diminished net surface radiation flux. The net effect of the westerly wind burst on the ocean surface heat and freshwater budgets is substantial cooling (the net heat flux varies between 0 and −100 W m^{-2}) and freshening ($P − E$ values ranging from 15 to 40 mm day^{-1}).

TABLE 3. Satellite-derived fluxes for the TOGA COARE averaged over the IFA during the IOP (maximum and minimum values refer to IFA-averaged, 3-hourly values). Positive values indicate flux into the ocean.

	Mean	Std dev	Max	Min
Heat flux (W m^{-2})				
Q_{rad}	176	279	839	−63
Q_{SH}	−5	5	0	−25
Q_{LH}	−120	42	−41	−254
Q_{PR}	−2	3	0	−26
Q_{net}	49	281	749	−312
Freshwater flux (mm day^{-1})				
P	8.3	15.0	237.8	0
E	4.2	1.5	8.8	1.4
F	4.1	14.5	232.6	−6.7
Momentum flux (N m^{-2})				
τ_a	5.6×10^{-2}	4.5×10^{-2}	2.7×10^{-1}	4.3×10^{-3}
τ_p	4.5×10^{-4}	8.8×10^{-4}	1.2×10^{-2}	0.0
M	5.7×10^{-2}	4.6×10^{-2}	2.7×10^{-1}	4.3×10^{-3}

During mid-January through the end of February, the IFA was characterized by short-lived high-amplitude wind events.

a. Net surface heat flux

Several studies have examined the total heat flux over parts of the IOP using in situ observations (e.g., Weller and Anderson 1996; Godfrey et al. 1998). Estimates of the IOP-averaged net surface heat flux made from in situ measurements near the IMET buoy (Fig. 1) range from 10 to 20 W m^{-2}, with estimates from mean ocean heat budgets within 10 W m^{-2} of the ship values. The IFA-averaged value of the net surface heat flux derived from satellite observations (Table 3) is significantly higher than the ship and buoy averages. Discrepancies may be caused by bias in the surface-based flux observations, errors in the satellite-derived

values, or differences in spatial coverage. Based upon coincident comparison of ship and buoy measurements, Godfrey et al. (1998) cite differences in net heat flux of 7 W m^{-2}. An estimate of ship and buoy bias errors obtained by summing biases of individual heat flux components (from section 4a) is 11 W m^{-2}. Biases in the net surface radiation fluxes from in situ measurements are likely to exceed the values cited by Weller and Anderson (1996), and it is plausible that the bias in the in situ measurements of net surface heat flux may exceed 20 W m^{-2} (see section 4a). We note here that use of the tuned Chou et al. (1998) values of downwelling shortwave and longwave fluxes only reduces the mean net satellite-derived heat flux by about 20–29 W m^{-2}, still significantly higher than the estimates from the buoys and ships.

The location of the R/V *Moana Wave,* R/V *Franklin,* R/V *Wecoma,* and the IMET buoy, upon which the surface-based estimates of the net heat flux are based, were typically within 1° of the IMET buoy location at 1°45′S, 156°E. To assess whether the smaller region measured by in situ observations was representative of the IFA, Fig. 7 shows a map of the satellite-derived net surface heat flux averaged over the IOP. Substantial spatial variations in IOP-averaged net surface heat fluxes are seen, with values in the western part of the domain being nearly twice as large as those in the eastern part of the domain. The value of the net heat flux determined from satellite for the grid cell nearest the IMET buoy is 37 W m^{-2}, somewhat lower than the domain average but still significantly larger than estimates from in situ measurements of 10–20 W m^{-2}. In fact, the sum of the bias errors for the satellite-derived surface heat flux components is −19 W m^{-2} (Table 1).

The satellite-based values of the net surface heat flux have a bias error that is the same magnitude as the net flux; however, there are still unresolved uncer-
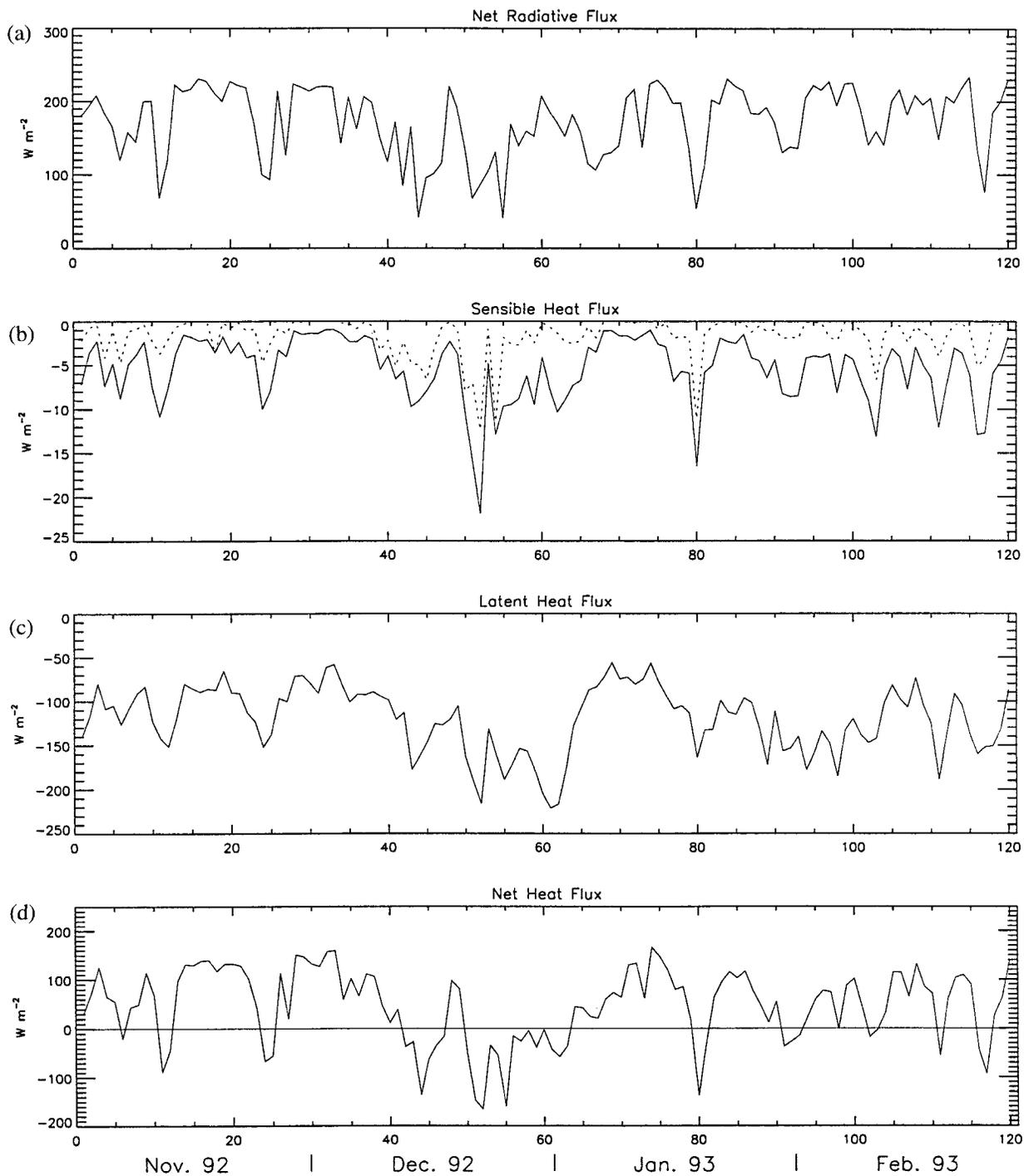
FIG. 4. Time series of daily averaged values averaged over the IFA of (a) net radiative flux, (b) sensible heat flux (solid) and sensible heat flux due to precipitation (dash), (c) latent heat flux, and (d) net heat flux.

tainties in both the in situ measurements and the satellite determinations. Further work (on going) may reduce the biases somewhat. The relatively high time correlations suggest that the satellite-based results are successfully representing the space and time variations of the fluxes. Since there is substantial space and time variability in the satellite results, point measurements should probably not be extrapolated spatially in the
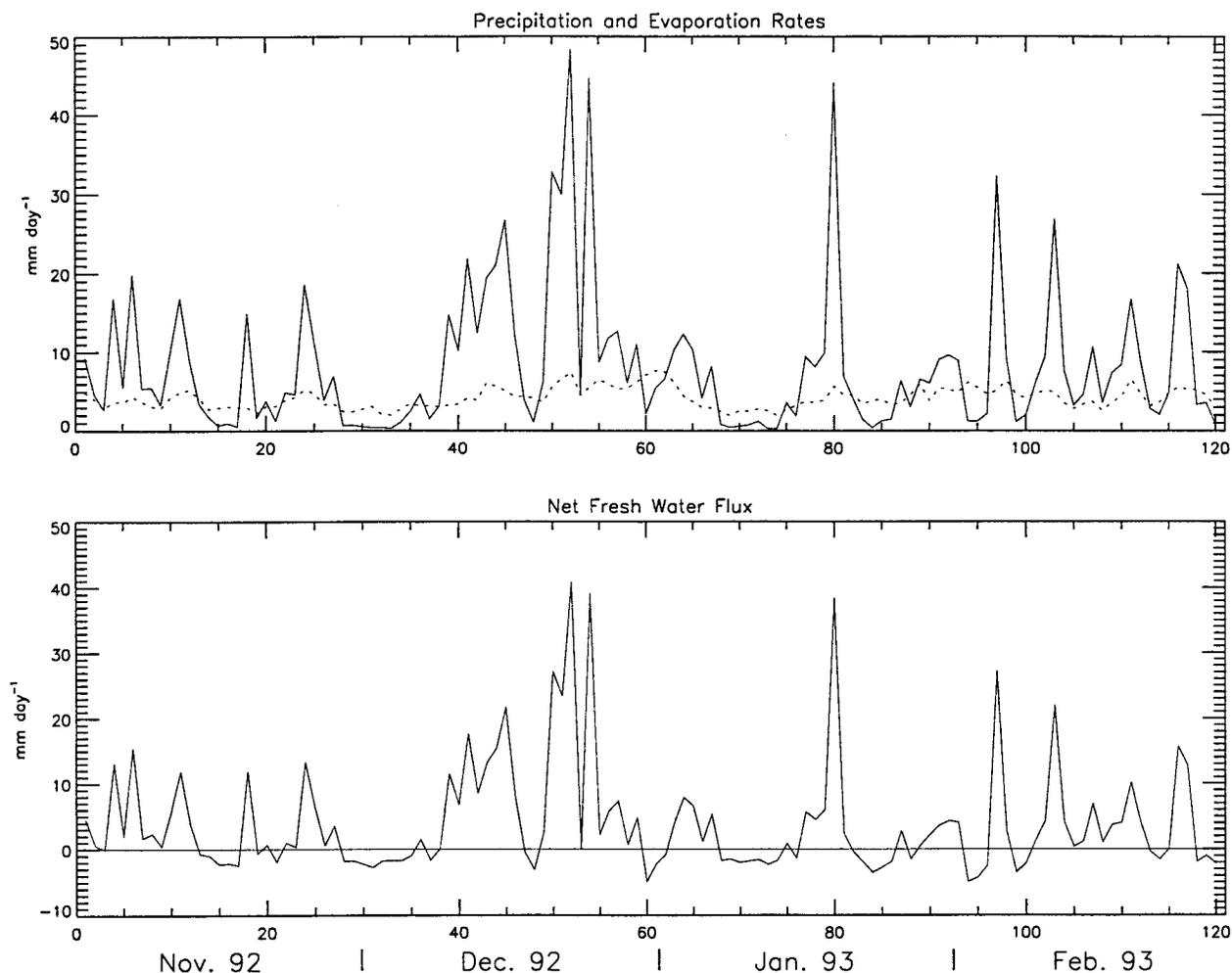
FIG. 5. Time series of daily averaged values averaged over the IFA of (top) precipitation (solid) and evaporation (dash), and (bottom) net freshwater flux.

tropical western Pacific. An important test of the satellite-derived heat flux values and their required accuracy would be to force a 3D ocean model with the observed flux fields.

b. Freshwater balance

Examination of Table 3 shows that daily values of precipitation when averaged over the IFA exceed evaporation by slightly more than a factor of 2, consistent with existing climatologies (e.g., Donguy 1987). IFA-averaged values of $P - E$ for the IOP are $8.3 - 4.2 = 4.1$ mm day^{-1}. These values compare favorably with values inferred by the R/V *Wecoma* (Feng et al. 1998) during the IOP of $P = 8$ mm day^{-1}, $E = 3.8$ mm day^{-1}, and $P - E = 4.1$ mm day^{-1}, where precipitation was determined as a residual of measured values of E and a determination of the salt budget of the ocean mixed layer.

Daily variations of IFA-averaged values of components of the surface freshwater flux are shown in Fig. 5. Although the IOP-averaged values of precipitation exceed evaporation by greater than a factor of 2, there are daily averaged periods as long as a week, averaged over the IFA, where evaporation slightly exceeds precipitation, resulting in a negative freshwater flux. During the peak period of the westerly wind burst (days 50–55), the IFA-averaged net freshwater flux reached 40 mm day^{-1}.

c. Comparison with integral budgets of heat, moisture, and moist static energy

A further analysis that can be done with the satellite-derived surface flux data is to compare the IFA-averaged surface flux values with vertical integrals of heat, moisture, and moist static energy budgets obtained from the TOGA COARE sounding
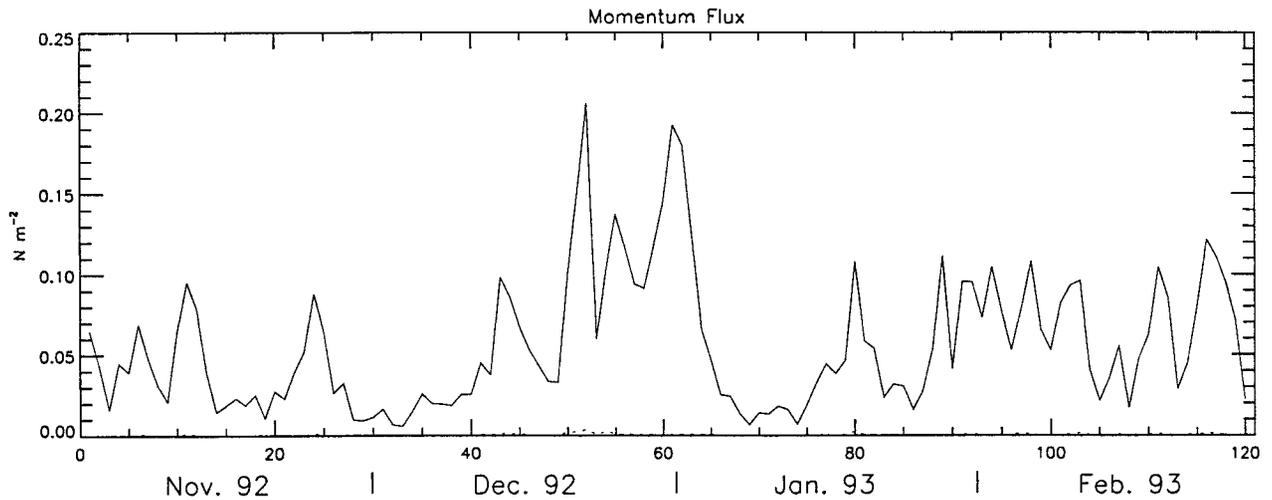
FIG. 6. Time series of daily averaged values averaged over the IFA of turbulent momentum flux (solid) and momentum flux due to rain (dash).

network. Following Yanai et al. (1973), we write the following equations for the vertical integrals of the heat, moisture, and moist static energy budgets:

$$\langle Q_1 \rangle = \langle Q_R \rangle + LP - Q_{SH} \qquad (7)$$

$$\langle LQ_2 \rangle = LP + Q_{LH} \qquad (8)$$

$$\langle Q_1 \rangle - \langle LQ_2 \rangle = \langle Q_R \rangle - (Q_{SH} + Q_{LH}), \qquad (9)$$

where Q_1 is the apparent heat source (total derivative of moist static energy), Q_2 is the apparent moisture sink (minus the total derivative of specific humidity), and

$$\langle \ \rangle \equiv \frac{1}{g} \int_T^0 (\ ) \, dp.$$

Values of Q_1 and Q_2 were obtained by performing computations using rawinsonde profiles at 6-h intervals throughout the IOP (Lin and Johnson 1996a). Note that we employ the oceanographic sign convention for the sensible and latent heat fluxes, whereby the fluxes are positive if there is heat going into the ocean. The integrated heating rate due to radiation was determined from the ISCCP-derived radiation information as

$$\langle Q_R \rangle = Q_T^{rad} - Q_0^{rad}, \qquad (10)$$

where the subscripts 0 and T correspond, respectively, to the surface and tropopause heights (here taken to be 100 hPa). The value of Q^{rad} at 100 hPa is determined from the same radiative transfer calculation using

ISCCP data that was used to determine the surface radiation flux. Equations (7)–(9) put powerful constraints on the surface fluxes, and comparison of the integral Q_1 and Q_2 values with the fluxes can help evaluate their accuracy.

Table 4 shows the evaluation of the heat, moisture, and moist enthalpy fluxes from (7)–(9), averaged over the TOGA COARE IFA during the IOP. Mismatches between the values on the right- and left-hand sides of the equations indicate discrepancies between the sounding-derived values of Q_1 and Q_2 and the
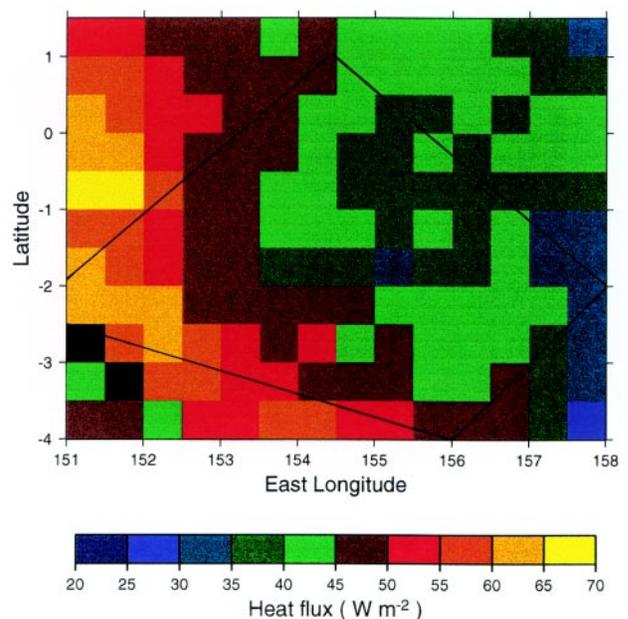

FIG. 7. Map over the IFA of net surface heat flux for the TOGA COARE IOP.

TABLE 4. Values of the IOP- and IFA-averaged budgets of heat, moisture, and moist enthalpy as per Eqs. (7)–(9).

	Eq.	Left-hand side (W m^{-2})	Right-hand side (W m^{-2})
$Q_1 = Q_R + LP - Q_{SH}$	(7)	216	165
$LQ_2 = LP + Q_{LH}$	(8)	129	119
$Q_1 - LQ_2 = Q_R - (Q_{SH} + Q_{LH})$	(9)	87	46

satellite-derived values of the fluxes. The moisture budget is within 10 W m^{-2} of balancing, while the heat and moist enthalpy budgets show an average imbalance of 51 and 41 W m^{-2}, respectively. Based on Table 1, most of the imbalance in the heat budget could be accounted for by the ~34 W m^{-2} bias in the satellite-based net surface radiative fluxes. Comparing the same type of calculations for a period when Earth Radiation Budget Experiment data are available indicates that the top-of-atmosphere fluxes probably contribute less than 10 W m^{-2} to this bias.

Figure 8 shows the time series of daily averaged values of the terms on the right- and left-hand sides of the heat, moisture, and moist static energy budget equations (7)–(9). Examination of the heat budget in Fig. 8a shows that the bias evident in the mean budgets does not arise from a systematic bias but from differences during several short periods. Considering the moisture budget (Fig. 8b), it is seen that not only do the mean values show good agreement, but that the magnitude of the variations is similar. Note that the periods of greatest discrepancies in both the heat and moisture budgets are frequently the same. While the mean imbalances in both the heat and moist enthalpy budgets are nearly the same magnitude, the amplitude of the variations in the moist static energy budget (Fig. 8c) is much greater for the left- rather than for the right-hand side of the equation (which is not seen in the heat budget).

Imbalances in the budgets of heat, moisture, and moist enthalpy can arise from errors in the satellite-derived fluxes and from the Q_1 and Q_2 budgets determined from the rawinsondes. Substantial problems with the TOGA COARE soundings have been identified by Lucas and Zipser (1996). Johnson and Ciesielski (1999) estimate that these errors are likely to result in a 10% error in $<Q_1>$ and a 3% error in $<Q_2>$. Reanalysis of the TOGA COARE soundings is under way, along with recalculation of Q_1 and Q_2 val-

ues. Additional errors in the Q_1 and Q_2 budgets arise from sampling and analysis methods (Lin and Johnson 1996b). The large amplitude variations on the left-hand side of the moist static energy budget suggest correlated errors in the Q_1 and Q_2 budgets.

Closing the atmospheric heat and moisture budgets for the IFA is essential for numerous applications, including an independent check on the large-scale average surface flux values and for providing an internally consistent dataset for modeling and diagnostic studies. It appears that at present, the heat budget over the IFA cannot be regarded as closed to better than about 20%, with the errors in the Q_1 and Q_2 values very possibly being greater than those in the satellite-derived surface flux components. It is anticipated that continued refinements of the satellite radiative flux algorithms and the sounding data will close the gap in the budgets. The major challenge will then be to reconcile the atmospheric budgets with oceanic budgets using the same surface flux dataset.

6. Conclusions

An integrated approach has been introduced for determining from satellite the tropical ocean surface turbulent fluxes of heat, moisture, and momentum at higher frequencies and spatial resolution than has been reported previously. A unique feature of this analysis is that we have attempted to obtain fluxes every 3 h, even when some of the conditions for direct retrieval are not met and when necessary satellite data are not available (e.g., use of polar orbiters). Improvements relative to previous efforts to remotely sense the surface fluxes include the use of higher space and time resolutions, improved cloud characteristics, a sophisticated radiative transfer model, and an improved bulk model for turbulent fluxes. By recognizing the physical relationship between various components of the
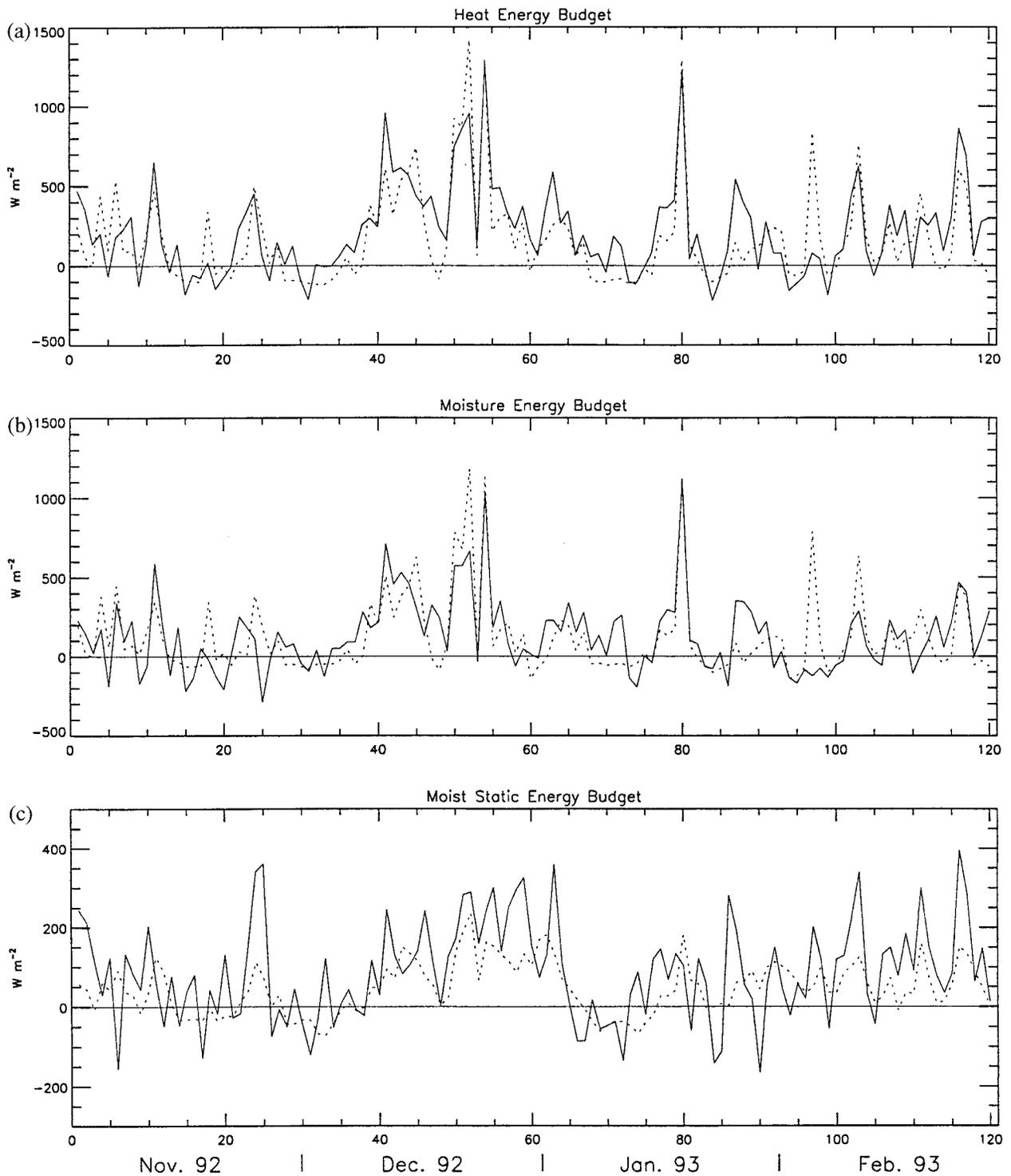
FIG. 8. Time series (daily averaged values) over the IFA of integral (a) heat, (b) moisture, and (c) moist static energy budgets. Solid lines indicate the values on the left-hand side of Eqs. (7)–(9) (including Q_1 and Q_2 values) and dotted lines indicate the values on the right-hand side of Eqs. (7)–(9) determined from the satellite-derived surface fluxes.

ocean–atmosphere system, and by taking advantage of the manner in which these variables are related, improved and physically self-consistent fluxes can be determined.

The validity of the satellite-derived surface fluxes and input parameters are examined using in situ measurements made from ships and aircraft in the western equatorial Pacific Ocean during TOGA COARE.

Pixel-scale comparisons of the satellite fluxes with the ship fluxes show biases that are somewhat larger than the estimated bias errors of the ship measurements but root-mean-square errors for the various component fluxes are smaller than or nearly equal to the standard deviation of the ship fluxes. The greatest bias of the satellite-derived surface fluxes relative to the in situ measurements is associated with the shortwave radiation fluxes; however, significant uncertainties remain in the in situ observations of the surface shortwave radiation fluxes. One of the greatest uncertainties in the calculation of the shortwave radiation fluxes from satellite observations is uncertainty about the amount and absorptivity of the aerosols in the Tropics. Some evidence suggests that biomass burning may be more prevalent than suspected, producing much more absorbing aerosol than assumed in our calculations.

Values of the satellite-derived surface fluxes when averaged over the IFA show greater values of average net surface heat flux than were obtained from in situ measurements in the center of the IFA. The satellite-derived fluxes show considerable spatial variability, although the location of the in situ measurements showed satellite-derived values of the net surface heat flux that were within about 10 W m^{-2} of the IFA-averaged satellite value. Discrepancies in the vertically integrated atmospheric heat budget of 50 W m^{-2} (about 20%) were determined. Although errors in the in situ measurements of net surface heat flux and the vertically integrated atmospheric heat budget may be substantial, the discrepancies in comparing both with the satellite-derived fluxes point to a high bias in the net surface heat flux as determined from satellite. Further improvement to the radiative transfer model and specification of cloud and aerosol optical properties are likely to lower the net surface radiation flux somewhat, but not enough to eliminate the discrepancy, some of which may be associated with errors in the in situ measurements and the vertically integrated atmospheric heat and moisture budgets. A definitive test of the satellite-derived surface flux dataset will be to balance successfully both the atmospheric budgets and oceanic budgets in the IFA using the same surface flux dataset.

Fields of surface fluxes derived from satellite fluxes on the time–space scales addressed in this paper will have application to atmospheric heat and moisture budget studies, forcing for 3D ocean models, validation of 3D atmospheric and coupled atmosphere–ocean models, and diagnostic studies related to sea surface temperature and feedbacks between the atmosphere and ocean. Satellite remote sensing techniques that have been validated by the TOGA COARE IOP data can then be used to determine surface fluxes over extended periods and over the global tropical oceans. Caution should be used in extending these algorithms outside of the tropical regions, since algorithms for surface wind speed, temperature, and humidity, as well as the sea surface temperature, have been formulated specifically for tropical conditions.

References

Atlas, R., R. Hoffman, S. Bloom, J. Jusem, and J. Ardizzone, 1996: A multiyear global surface wind velocity dataset using SSM/I wind observations. *Bull. Amer. Meteor. Soc.,* **77,** 869–882.

Bishop, J. K. B., and W. B. Rossow, 1991: Spatial and temporal variability of global surface solar irradiance. *J. Geophys. Res.,* **96,** 16 839–16 858.

Bush, B. C., F. P. J. Valero, A. S. Simpson, and L. Bignone, 1999: Characterization of thermal effects in pyranometers: A data correction algorithm for improved measurement of surface insolation. *J. Atmos. Oceanic Technol.,* in press.

Caldwell, D. R., and W. P. Elliott, 1971: Surface stresses produced by rainfall. *J. Phys. Oceanogr.,* **1,** 145–148.

Chou, M. D., Q. Zhao, and S. H. Chou, 1998: Radiation budgets and cloud radiative forcing in the Pacific warm pool during TOGA COARE. *J. Geophys. Res.,* **103,** 16 967–16 977.

Chou, S. H., C. L. Shie, R. M. Atlas, and J. Ardizzone, 1997: Air–sea fluxes retrieved from special sensor microwave imager data. *J. Geophys. Res.,* **102,** 12 705–12 726.

Clayson, C. A., and J. A. Curry, 1996: Determination of surface turbulent fluxes for the Tropical Ocean–Global Atmosphere Coupled Ocean–Atmosphere Response Experiment: Comparison of satellite retrievals and in situ measurements. *J. Geophys. Res.,* **101,** 28 515–28 528.

——, C. W. Fairall, and J. A. Curry, 1996: Evaluation of turbulent fluxes at the ocean surface using surface renewal theory. *J. Geophys. Res.,* **101,** 28 503–28 514.

Donguy, J.-R., 1988: Recent advances in the knowledge of the climatic variations in the tropical Pacific Ocean. *Prog. Oceanogr.,* **19,** 49–85.

Ebert, E. E., and M. J. Manton, 1998: Performance of satellite rainfall estimation algorithms during TOGA COARE. *J. Atmos. Sci.,* **55,** 1537–1557.

Fairall, C. W., E. F. Bradley, D. P. Rogers, J. B. Edson, and G. S. Young, 1996a: Bulk parameterization of air–sea fluxes for Tropical Ocean–Global Atmosphere Coupled Ocean–Atmosphere Response Experiment. *J. Geophys. Res.,* **101,** 3747–3764.

——, ——, J. S. Godfrey, J. B. Edson, G. S. Young, and G. A. Wick, 1996b: Cool-skin and warm-layer effects on sea surface temperature. *J. Geophys. Res.,* **101,** 1295–1308.

——, A. B. White, and J. E. Hare, 1997: Integrated shipboard measurements of the marine boundary layer. *J. Atmos. Oceanic Technol.,* **14,** 338–359.

Feng, M., P. Hacker, and R. Lukas, 1998: Upper ocean heat and salt balances in response to a westerly wind burst in the western equatorial Pacific during TOGA COARE. *J. Geophys. Res.,* **103,** 10 289–10 311.

Gautier, C., R. Frouin, and J.-Y. Simonot, 1988: An attempt to remotely sense from space the surface heat budget over the Indian Ocean during the 1979 monsoon. *Geophys. Res. Lett.,* **15,** 1121–1124.

Geldmeier, M. F., and G. M. Barnes, 1997: The "footprint" under a decaying tropical mesoscale convective system. *Mon. Wea. Rev.,* **125,** 2879–2895.

Godfrey, J. S., R. A. Houze Jr., R. H. Johnson, R. Lukas, J.-L. Redelsperger, A. Sumi, and R. Weller, 1998: Coupled Ocean–Atmosphere Response Experiment (COARE): An interim report. *J. Geophys. Res.,* **103,** 14 395–14 450.

Gosnell, R., C. W. Fairall, and P. J. Webster, 1995: The surface sensible heat flux due to rain in the tropical Pacific Ocean. *J. Geophys. Res.,* **100,** 18 437–18 442.

Han, Q., W. B. Rossow, and A. A. Lacis, 1994: Near-global survey of effective droplet radii in liquid water clouds using ISCCP data. *J. Climate,* **7,** 465–497.

Hansen, J., M. Sato, and R. Ruedy, 1997: Radiation forcing and climate response. *J. Geophys. Res.,* **102,** 6831–6864.

Hayes, S. P., M. J. McPhaden, and A. Leetmaa, 1989: Observational verification of a quasi real time simulation of the tropical Pacific Ocean. *J. Geophys. Res.,* **94,** 1346–1356.

Hollinger, J., J. Peirce, and G. Poe, 1990: Validation for the Special Sensor Microwave/Imager (SSM/I). *IEEE Trans. Geosci. Remote Sens.,* **28,** 781–790.

Jabouille, P., J. L. Redelsperger, and J. P. Lafore, 1996: Modification of surface fluxes by atmospheric convection in the TOGA COARE region. *Mon. Wea. Rev.,* **124,** 816–837.

Johnson, R. H., and P. E. Ciesielski, 1999: Rainfall and radiative heating rate estimates from TOGA COARE atmospheric budgets. *J. Atmos. Sci.,* in press.

——, ——, and K. A. Hart, 1996: Tropical inversions near the 0°C level. *J. Atmos. Sci.,* **53,** 1838–1855.

Katsaros, K. B., and J. E. DeVault, 1986: On irradiance measurement errors at sea due to tilt of radiometers. *J. Atmos. Oceanic Technol.,* **3,** 740–745.

Lin, X., and R. H. Johnson, 1996a: Kinematic and thermodynamic characteristics of the flow over the western Pacific warm pool during TOGA COARE. *J. Atmos. Sci.,* **53,** 695–715.

——, and ——, 1996b: Heating, moistening, and rainfall over the western Pacific warm pool during TOGA COARE. *J. Atmos. Sci.,* **53,** 3367–3383.

Liu, G., J. A. Curry, and R. S. Sheu, 1995: Classification of clouds over the western equatorial Pacific Ocean using combined infrared and microwave satellite data. *J. Geophys. Res.,* **100,** 13 811–13 824.

Lucas, C., and E. Zipser, 1996: The variability of vertical profiles of wind, temperature and moisture during TOGA COARE. Preprints, *Seventh Conf. on Mesoscale Processes,* Reading, United Kingdom, Amer. Meteor. Soc., 125–127.

Ma, Q., and R. H. Tipping, 1994: The detailed balance requirement and general empirical formalisms for continuum absorption. *J. Quant. Spectr. Radiat. Transf.,* **51,** 751–757.

McClain, E. P., W. G. Pichel, and C. C. Walton, 1985: Comparative performance of AVHRR-based multichannel sea surface temperatures. *J. Geophys. Res.,* **90,** 11 587–11 601.

Michael, K. J., and M. Nunez, 1991: Derivation of ocean–atmosphere heat fluxes in a tropical environment using satellite and surface data. *Int. J. Climatol.,* **11,** 559–575.

Miller, D. K., and K. B. Katsaros, 1992: Satellite-derived surface latent heat fluxes in a rapidly intensifying marine cyclone. *Mon. Wea. Rev.,* **120,** 1093–1107.

Pinker, R. T., and J. A. Ewing, 1985: Modeling surface solar radiation: Model formulation and validation. *J. Climate Appl. Meteor.,* **24,** 389–401.

Reynolds, R. W., and D. C. Marsico, 1993: An improved real-time global SST analysis. *J. Climate,* **6,** 114–119.

Rossow, W. B., and Y.-C. Zhang, 1995: Calculation of surface and top-of-atmosphere radiative fluxes from physical quantities based on ISCCP datasets, Part II: Validation and first results. *J. Geophys. Res.,* **100,** 1167–1197.

——, and R. A. Schiffer, 1999: Advances in understanding clouds from ISCCP. *Bull. Amer. Meteor. Soc.,* in press.

——, A. W. Walker, D. Beuschel, and M. Roiter, 1996: International Satellite Cloud Climatology Project (ISCCP): Description of new cloud datasets. WMO/TD-No. 737, World Climate Research Programme (ICSU and WMO), Geneva, Switzerland, 115 pp. [Available from World Climate Research Programme, 41 Avenue Giuseppe-Motta, CP 2300, 1211 Geneva 2, Switzerland.]

Schluessel, P., and W. J. Emery, 1990: Atmospheric water vapour over oceans from SSM/I measurements. *Int. J. Remote Sens.,* **11,** 753–766.

——, ——, H. Grassl, and T. Mammen, 1990: On the bulk-skin temperature difference and its impact on satellite remote sensing of sea surface temperature. *J. Geophys. Res.,* **95,** 13 341–13 356.

Schulz, J., J. Meywerk, S. Ewald, and P. Schlüssel, 1997: Evaluation of satellite-derived latent heat fluxes. *J. Climate,* **10,** 2782–2795.

Sheu, R.-S., and G. Liu, 1995: Atmospheric humidity variations associated with westerly wind bursts during TOGA COARE. *J. Geophys. Res.,* **100,** 25 759–25 768.

——, J. A. Curry, and G. Liu, 1996: Satellite retrieval of tropical rainfall using ISCCP analyses and microwave measurements. *J. Geophys. Res.,* **101,** 21 291–21 301.

Smith, E. A., and Coauthors, 1998: Results of WetNet PIP-2 project. *J. Atmos. Sci.,* **55,** 1483–1536.

Suomi, V. E., L. A. Sromovsky, and J. R. Anderson, 1996: Measuring ocean–atmosphere heat flux with a new in situ sensor. Preprints, *Eighth Conf. on Air–Sea Interaction,* Atlanta, GA, Amer. Meteor. Soc., 38–42.

Webb, E. K., G. I. Pearman, and R. Luening, 1980: Correction of flux measurements for density effects due to heat and water vapour transfer. *Quart. J. Roy. Meteor. Soc.,* **106,** 85–100.

Webster, P. J., and R. Lukas, 1992: TOGA COARE: The Coupled Ocean–Atmosphere Response Experiment. *Bull. Amer. Meteor. Soc.,***73,** 1377–1416.

——, C. A. Clayson, and J. A. Curry, 1996: Clouds, radiation, and the diurnal cycle of sea surface temperature in the tropical western Pacific. *J. Climate,* **9,** 1712–1730.

Weller, R. A., and S. P. Anderson, 1996: Surface meteorology and air–sea fluxes in the western equatorial Pacific warm pool during the TOGA Coupled Ocean–Atmosphere Response Experiment. *J. Climate,* **9,** 1959–1990.

Wick, G. A., W. J. Emery, and P. Schluessel, 1996: The behavior of bulk-skin sea surface temperature difference under varying wind speed and heat flux. *J. Phys. Oceanogr.,* **26,** 1969–1988.

Yanai, M., S. Esbensen, and J. H. Chu, 1973: Determination of bulk properties of tropical cloud clusters from large-scale heat and moisture budgets. *J. Atmos. Sci.,* **30,** 611–627.

Young, G. S., S. M. Perugini, and C. W. Fairall, 1995: Convective wakes in the equatorial western Pacific dufing TOGA. *Mon. Wea. Rev.,* **123,** 110–123.

Zhang, Y.-C., W. B. Rossow, and A. A. Lacis, 1995: Calculation of surface and top-of-atmosphere radiative fluxes from physical quantities based on ISCCP datasets, Part I: Method and sensitivity to input data uncertainties. *J. Geophys. Res.,* **100,** 1149–1165.